This article has been accepted for publication in a future issue of this journal, but has not been fully edited. Content may change prior to final publication. Citation information: DOI 10.1109/TCSVT.2021.3114601, IEEE Transactions on Circuits and Systems for Video Technology

Single Image Haze Removal Based on a Simple Additive Model with Haze Smoothness Prior

Xiaoqin Zhang *Member, IEEE,* Tao Wang, Guiying Tang, Li Zhao,
Yuewang Xu, Stephen Maybank *Fellow, IEEE,*

***Abstract*—Single image haze removal, which is to recover the clear version of a hazy image, is a challenging task in computer vision. In this paper, an additive haze model is proposed to approximate the hazy image formation process. In contrast with the traditional optical model, it regards the haze as an additive layer to a clean image. The model thus avoids estimating the medium transmission rate and the global atmospherical light. In addition, based on a critical observation that haze changes gradually and smoothly across the image, a haze smoothness prior is proposed to constrain this model. This prior assumes that the haze layer is much smoother than the clear image. Benefiting from this prior, we can directly separate the clean image from a single hazy image. Experimental results and comparisons with synthetic images and real-world images demonstrate that the proposed method outperforms state-of-the-art single image haze removal algorithms.**

I. Introduction

Images captured outdoors are affected by liquid droplets or small dust particles in the air, collectively known as aerosols. These aerosols absorb the light from the atmosphere and scatter the light reflected from objects in the field of view. These phenomena lead to hazy images, which often suffer from low contrast, faint regions, and color shift. These effects limit the visual quality of images and greatly hinder outdoor computer vision and image processing algorithms. Therefore, research on haze removal is essential.

Dehazing is an increasingly desirable technique in a variety of computational photography and computer vision tasks. A haze optical model was proposed in 1924 [1]. However, haze removal based on this model is an under-constrained problem for single image input. More information is required to perform image dehazing.

Researchers first consider utilizing multiple images to dehaze. Naturally, multiple images can provide more information than a single image input. In [2, 3], images taken with different degrees of polarization are used to dehaze. In [4–6], Narasimhan and Nayar propose haze removal approaches with multiple images of the same scene captured in different weather conditions. But it is difficult to obtain multiple images in practical applications, such as video surveillance and assisted driving. Therefore, single image dehazing has attracted more and more attention in recent years.

X. Zhang, T. Wang, G. Tang, L. Zhao and Y. Xu are with the Department of Computer Science, Wenzhou University, 325035, China (e-mail: zhangxiaoqinnan@gmail.com, taowangzj@gmail.com, guiyingtang9503@163.com, lizhao@wzu.edu.cn, yuewangxu221@gmail.com).
S. Maybank is with the School of Computer Science and Information Systems, Birkbeck College, WC1E7HX, U.K. (e-mail: sjmaybank@dcs.bbk.ac.uk).

Researchers have focused on single image dehazing over the past decade. Existing single image dehazing methods can be broadly classified into three categories: methods based on adaptive contrast enhancement, methods based on transmission estimation, and methods based on neural networks. Brief reviews of these methods are given in the following paragraphs.

Methods based on adaptive contrast enhancement can realize the dehazing of a single image. Fattal proposes a dehazing method using independent component analysis [7]. It requires sufficient color information and image variation, but it performs poorly on images taken in dense fog. Tan implements single image dehazing by maximizing the contrast per patch [8]. However, the method suffers from artifacts, over-saturation, and high computational complexity. In [9], the authors present a dehazing algorithm based on a prediction model. However, the results are subject to severe over-saturation. The method in [10] extends a well-known perception-inspired variational framework to achieve single image dehazing. In [11], the image is segmented into regions containing relatively small variations in depth. The contrast is stretched within each region, but this may lead to artifacts at the boundaries between regions.

Methods based on transmission estimation are very popular. They usually depend on the aforementioned optical model For instance, He *et al*. [12] find that most outdoor objects in clear weather have at least one color channel that is significantly darker than the other channels. This phenomenon is named dark channel prior (DCP). Nevertheless, it is computationally intensive and unreliable when handling sky regions that contain white parts. Many improved algorithms [13–18] have emerged to overcome these shortcomings by replacing the time-consuming soft matting in [12] with a fast median filter [19] (a fast visibility restoration method, we call it FVR for short), standard median filter [14], "median" of median filter [20], and guided image filter [21]. Meng *et al*. [22] further explore region boundary constraints and contextual regularization (BCCR) based on the dark channel prior and obtain better restoration. However, over-enhancement may still occur. And a newly proposed channel-weighted analysis [23] aims to eliminate the unnatural effect of DCP method. Another two approaches based on hue disparity prior and color attenuation prior are proposed by Ancuti *et al*. [24] and Zhu *et al*. [25], respectively. The former approach is not robust and often suffers from large errors because of ambiguities in assessing color and depth. The latter approach proposes a new effective color attenuation prior (CAP), and creates a linear model for modeling the scene depth of the

This article has been accepted for publication in a future issue of this journal, but has not been fully edited. Content may change prior to final publication. Citation information: DOI 10.1109/TCSVT.2021.3114601, IEEE Transactions on Circuits and Systems for Video Technology

hazy image under this novel prior. Although it needs to be trained in advance, it outperforms other methods except for some methods based on neural networks, as described in a recent review article [26]. A Bayesian defogging (BD) method is introduced in [27] to estimate scene radiance and scene depth. The random field is used in a preliminary step to obtain the transmission. However, the restored images are often over-saturated and distorted. The authors in [9] propose a referenceless prediction (this approach is named DEFADE by authors), which restores the details in hazy images very well, but its results suffer from over-saturation. On account of the observation that pixels in a haze-free image from color-lines in RGB space, Fattal proposes to use color lines for dehazing [28]. Inspired by color-lines, Berman *et al*. propose a non-local dehazing (NLD) method in [29] and introduce a new conception of haze lines in 2016 and modified their work in the following year [30]. Based on reformulation of the traditional optical model, a convex optimization (CO) algorithm is introduced to achieve fast haze removal in [31]. Methods for suppressing artifacts are studied in [32] and [33]. The former paper focuses on block artifacts that are usually caused by compression (we call this work JPEG for short) and the latter paper utilizes the gradient residual minimization (GRM) to suppresses edges in the dehazed images that do not exist in the input images. Ju *et al*. [34] first propose a novel image prior called gamma correction prior (GCP). Then based on this prior and the atmospheric scattering model, a method named IDGCP is developed for single image dehazing. In [35], the authors introduce a new parameter (*i.e.* light absorption coefficient) into the atmospheric scattering model and it results an enhanced ASM (EASM). Based on the ESAM, they develop an image dehazing method called IDE. Zhang *et al*. [36] present a simple but effective image prior, called a maximum reflection prior, to estimate the varying ambient illumination and it can address a haze removal problem from a single nighttime image. Zhang *et al*. [37] propose a method called 3R to simulate nighttime hazy images from corresponding daytime ones. It first reconstructs the scene geometry, then simulates the light rays and object reflectance, and renders the haze effects in the end.

In recent years, learning-based algorithms [38–43] are also proposed for image dehazing. For example, a fast and accurate multi-scale end-to-end dehazing network called FAMED-Net is proposed in [41]. It directly recovers the clear image by encoders at three scales and a fusion module. Li *et al*. [39] adopt an end-to-end AOD-Net (here AOD represents All-in-One Dehazing), which integrates transmission and air-light into a new variable. The desired output is obtained directly from the input. Ren *et al*. [44] propose a multi-scale convolutional neural network (MSCNN) which first generates a coarse-scale transmission matrix and then gradually refines it. In [45], the authors present a trainable model for estimating the transmission matrix from a hazy image. A deep fully convolutional regression network (DFCRN) and gated context aggregation network (GCAN) for dehazing are presented in [46] and [47], respectively. [48] presents an efficient multi-scale correlated wavelet (MSCW) approach to solve the image dehazing problem in the frequency domain. Combining model-based and fusion-based dehazing methods, [49] utilizes multi-band fusion (MBF) method to extract the base and detail layers for intensity and Laplacian modules. Shao *et al*. [50] propose a domain adaptation image dehazing framework, which contains an image translation module and two image dehazing modules. These CNN-based methods produce promising dehazing results. However, the neural network is difficult to interpret and is strongly affected by the choice of training data. In this paper, we lay emphasis on the traditional method and compare several CNN methods meanwhile.

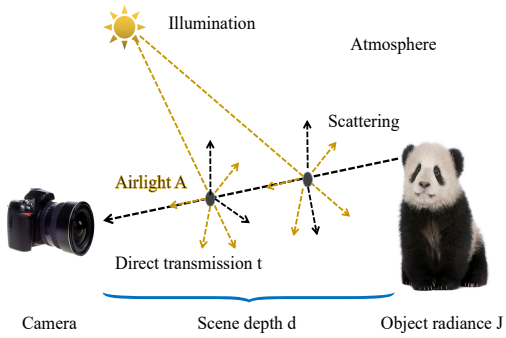

Fig. 1. Optical Model

This paper mainly introduces the following four contributions. **(I)** A new simple additive haze model is proposed. In this model, the hazy image is regarded as the sum of the clear image and corresponding haze layer. Compared with the common optical model, which involves both additive and multiplicative parts, the new model only includes an additive part and avoids estimating the medium transmission rate and global atmospheric light. **(II)** An effective haze smoothness prior is introduced and incorporated into the haze model to ensure the identifiability of the haze layer and the haze-free image layer. **(III)** We propose an effective single image haze removal algorithm whose convergence is guaranteed both theoretically and experimentally. **(IV)** The method in this paper has remarkable dehazing results and outperforms most state-of-the-art dehazing approaches.

The remainder of this paper is organized as follows. Section II gives a quick review of the primary optical model. The new method is presented in Section III. To illustrate the effectiveness of the proposed method, extensive experiments and comparisons are conducted in Section IV. Finally, Section V concludes the paper.

II. Optical Model

To make the paper self-contained, a quick review of the traditional optical model is provided. It is formulated as

$$I(x) = t(x)J(x) + A(1 - t(x)), \tag{1}$$

where x is the pixel coordinate in the image plane, I is the observed image which is degraded by haze, J denotes the object radiance, as measured in fine weather. The matrix A represents air light, and t is the medium transmission rate that describes the proportion of the light that reaches the camera without being scattered. The parameter t can be expressed as:

$$t(x) = e^{-\beta d(x)}, \tag{2}$$

This article has been accepted for publication in a future issue of this journal, but has not been fully edited. Content may change prior to final publication. Citation information: DOI 10.1109/TCSVT.2021.3114601, IEEE Transactions on Circuits and Systems for Video Technology

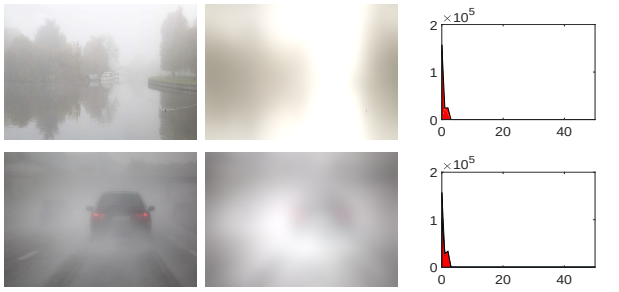

(a) Observed images (b) Haze layers (c) Gradient histograms

Fig. 2. A check of the validity of haze smoothness prior. From left to right: the observed hazy images, corresponding haze layers, and gradient histograms of haze layers. The horizontal and vertical coordinates of (c) are absolute values of gradient magnitude and corresponding numbers, respectively. To make the picture clearer, only the region 0-40 is shown.

where β is the scattering coefficient of the atmosphere. It is a constant if the atmosphere is homogeneous. d is scene depth, *i.e.,* the distance from the object to the camera.

The traditional optical model is illustrated in Fig. 1. The goal of dehazing is to recover J from the observed image I with A and t as by-products. This is a severely ill-posed problem.

III. Our Method

In this section, we first propose a novel additive model to describe the formation of a hazy image and then introduce a powerful haze smoothness prior to constrain it. The technical details are as follows.

A. Haze Formation Modeling

Inspired by the general image denoising model, we regard the haze in the observed image as additive noise and propose an additive model to approximate the hazy image formation. Formally, the hazy image is expressed as the addition of the clear image layer and the haze image layer:

$$I(x) = J(x) + H(x), \tag{3}$$

where J is the clear image to be recovered, and H is the haze layer that is added to the clear image. Our method is to separate the clear image J from the hazy image I.

Compared with the common optical model (1) which involves both additive and multiplicative parts, the new one includes an additive part only and avoids estimating the medium transmission rate t and global atmospheric light A, which affect a lot in the original model. However, this model is still under-constrained. More constraints on the model are required.

B. Haze Smoothness Prior

It is observed that the haze changes gradually and smoothly in natural images. Therefore, we make a reasonable assumption that the haze layer is smooth. As illustrated in Fig. 2, the histogram of gradient magnitudes obtained from the haze layer has a remarkably short tail. Most of the gradient magnitudes are near zero. Small gradient magnitudes are likely to occur in H, and larger gradient magnitudes are likely to occur in J. The haze smoothness prior assumes that the haze layer H is smoother than the clear image J. As shown in [51], we could encode this attribute into probability density functions as:

$$\begin{aligned} P_J(\nabla_x J) &= \frac{1}{w}\max\{e^{-\frac{\nabla_x^2 J}{2\sigma_1^2}}, \tau\}, \\ P_H(\nabla_x H) &= \frac{1}{\sqrt{2\pi}\sigma_2} e^{-\frac{\nabla_x^2 H}{2\sigma_2^2}}, \end{aligned} \tag{4}$$

where $\nabla_x J$ and $\nabla_x H$ denote gradient magnitudes at pixel x in J and H respectively, P_J and P_H are two probability density functions related to J and H respectively, and w is a normalization parameter. The $\max$ operator with the threshold value τ is used to prevent the probability density from approaching zero as the magnitude of the gradient becomes large. σ_1 and σ_2 are standard deviations of respective Gaussian distributions. According to the gradient sparsity prior [52], σ_2 should be smaller than σ_1 to ensure that the gradient distribution of H falls faster than that of J.

To recover J, we maximize the joint probability density functions $P_J(\nabla_x J)$ and $P_H(\nabla_x H)$ on condition that $J+H=I$. For convenience, we minimize the negative natural logarithm of it directly. That is,

$$\begin{aligned} &-\min \log(P_J(\nabla_x J)P_H(\nabla_x H)) \\ &\propto \min\{\frac{\nabla_x^2 J}{-2\sigma_1^2 \log \tau}, 1\} + \frac{\nabla_x^2 H}{2\sigma_2^2}. \end{aligned} \tag{5}$$

Minimization function (5) can be further simplified by replacing the inner $\min$ operator with $\rho(\nabla_x J) = \min\{\frac{\nabla_x^2 J}{k}, 1\}$ where the term k is a small positive value:

$$\begin{aligned} \min_{J,H} \ & \rho(\nabla_x J) + \lambda \nabla_x^2 H, \\ s.t. \ & J + H = I, \end{aligned} \tag{6}$$

where parameter λ contains the constants in function (5) and controls the smoothness of the haze layer. Since the degree of smoothness is very high, λ should be given a large value.

C. Dehazing Model

In our single image dehazing task, selecting proper gradient operators leads to the following dehazing model:

$$\begin{aligned} \min_{H,J} \ & \lambda \|f_{La} * H\|_F^2 + \sum_{i=1}^{2} \rho(f_i * J), \\ s.t. \ & J + H = I, \end{aligned} \tag{7}$$

where symbol $*$ denotes convolution operation, $\|\cdot\|_F$ represents the Frobenius norm, $f_1 = [-1, 1]$ is first order horizontal derivative filter, $f_2 = [-1, 1]^T$ is first order vertical derivative filter, and $f_{La} = \begin{bmatrix} 0 & 1 & 0 \\ 1 & -4 & 1 \\ 0 & 1 & 0 \end{bmatrix}$ is second order Laplacian filter. The formula of ρ is as defined before. It is worth noting that the first order gradient operators f_1 and f_2 help to preserve significant edges while the second order Laplacian filter f_{La} is isotropic and able to suppress smooth regions [53]. Then the dehazing model is obtained:

$$\min_{J} \lambda \|f_{La} * (I - J)\|_F^2 + \sum_{i=1}^{2} \rho(f_i * J). \tag{8}$$

This article has been accepted for publication in a future issue of this journal, but has not been fully edited. Content may change prior to final publication. Citation information: DOI 10.1109/TCSVT.2021.3114601, IEEE Transactions on Circuits and Systems for Video Technology

D. Optimization

To simplify problem (8), the auxiliary variables G_i $(i = 1, 2)$ are introduced. The minimization (8) is converted to the following form:

$$\min_{J,G} \lambda\|f_{La} * (I-J)\|_F^2 + \sum_{i=1}^{2}(\rho(G_i) + \alpha\|G_i - f_i * J\|_F^2), \quad (9)$$

where α is weight parameter. As α gets larger, the solution of function (9) gets closer to that of function (8). Since ρ is an approximation of the ℓ_0 norm [54] when the parameter k in ρ is sufficiently small. Therefore, ℓ_0 norm replaces ρ for solving easily.

$$\min_{J,G} \lambda\|f_{La} * (I-J)\|_F^2 + \sum_{i=1}^{2}(\|G_i\|_0 + \alpha\|G_i - f_i * J\|_F^2), \quad (10)$$

where $\|G_i\|_0$ stands for ℓ_0 norm of matrix G_i. Since optimizing J, G_1, and G_2 simultaneously in problem (8) could be expensive in practice, the half-quadratic separation (HQS) scheme is used to minimize it. Thus, problem (10) can be solved by an alternating optimization with respect to G_i and J. And the corresponding sub-problems in this process have closed-form solutions that can be obtained efficiently. The whole optimization process is summarized in the following:

Step1 Given $J^{(k)}$, update $G_i^{(k+1)}$ for $i = 1, 2$ by

$$\begin{aligned} &\arg\min_{G_i} \|G_i\|_0 + \alpha\|G_i - f_i * J^{(k)}\|_F^2 \\ =&\mathcal{H}_{\sqrt{\frac{1}{\alpha}}}(f_i * J^{(k)}), \end{aligned} \quad (11)$$

where $[\mathcal{H}_\mu(A)]_{i_1 i_2} = \begin{cases} [A]_{i_1 i_2}, & \text{if } |[A]_{i_1 i_2}| > \mu, \\ 0, & \text{otherwise.} \end{cases}$, $|\cdot|$ is absolute value, and $[A]_{i_1 i_2}$ stands for the entry which local in i_1-th column and i_2-th row of A. This solution holds while $\alpha < \frac{1}{k}$.

Step2 Given $G_i^{(k+1)}$ for $i = 1, 2$, update $J^{(k+1)}$ by

$$\arg\min_{J} \lambda\|f_{La} * (I-J)\|_F^2 + \alpha\sum_{i=1}^{2}\|f_i * J - G_i^{(k+1)}\|_F^2. \quad (12)$$

Note that the function being minimized in (12) is quadratic in J. The minimization is solved by:

$$\lambda f_{La}^T * (f_{La} * (J-I)) + \alpha\sum_{i=1}^{2} f_i^T * (f_i * J - G_i^{(k+1)}) = 0. \quad (13)$$

The equation (13) can be solved in the fast Fourier transform domain by applying a 2D Fast Fourier Transform (FFT) under the circular boundary condition. Then, we can compute J directly:

$$\begin{aligned} &J^{(k+1)} \\ &= F^{-1}\left(\frac{\alpha\sum_{i=1}^{2}(\overline{\mathcal{F}(f_i)}\mathcal{F}(G_i^{(k+1)})) + \lambda\overline{\mathcal{F}(f_{La})}\mathcal{F}(f_{La})\mathcal{F}(I)}{\alpha\sum_{i=1}^{2}(\overline{\mathcal{F}(f_i)}\mathcal{F}(f_i)) + \lambda\overline{\mathcal{F}(f_{La})}\mathcal{F}(f_{La}) + \varepsilon}\right), \end{aligned} \quad (14)$$

where $\mathcal{F}$ denotes FFT, $\bar{(\cdot)}$ represents the complex conjugate, and ε is a small constant for preventing division by 0. Unless indicated otherwise, all the foregoing calculations are performed in an element-wise manner. The detailed optimization process (HSP) is given in algorithm 1. And the corresponding convergence analysis is given in Conclusion 1.

Algorithm 1: HSP via HQS scheme

Input: Observed image I, λ, α, iteration number κ, tolerance τ, f_i for $i = 1, 2$ and f_{La}.

Initialization: $k = 1$, $J^{(1)} = I$ and $err = 0$.

while $err > \tau$ & $k < \kappa$ **do**

  // update $G_i^{(k+1)}$ using (10) for $i = 1, 2$;

  // update $J^{(k+1)}$ using (13);

  $k = k + 1$;

  $err = \frac{\|J^{(k+1)} - J^{(k)}\|_F^2}{\|J^{(k)}\|_F^2} + \sum_{i=1}^{2}\frac{\|G_i^{(k+1)} - G_i^{(k)}\|_F^2}{\|G_i^{(k)}\|_F^2}$;

end

Output: Dehazed image J.

Conclusion 1. *Set*

$$c(J, G_1, G_2) := \lambda\|f_{La} * (I-J)\|_F^2 + \sum_{i=1}^{2}(\|G_i\|_0 + \alpha\|G_i - f_i * J\|_F^2)$$

It follows that

$$c(J^{(k+1)}, G_1^{(k+1)}, G_2^{(k+1)}) \le c(J^{(k)}, G_1^{(k)}, G_2^{(k)}).$$

By the definition of $G_i^{(k+1)}$ for $i = 1, 2$,

$$\begin{aligned} &\|G_i^{(k+1)}\|_0 + \alpha\|G_i^{(k+1)} - f_i * J^{(k)}\|_F^2 \le \\ &\|G_i^{(k)}\|_0 + \alpha\|G_i^{(k)} - f_i * J^{(k)}\|_F^2, \end{aligned} \quad (15)$$

thus,

$$\begin{aligned} &c(J^{(k)}, G_1^{(k+1)}, G_2^{(k+1)}) \\ =&\lambda\|f_{La} * (I - J^{(k)})\|_F^2 + \sum_{i=1}^{2}(\|G_i^{(k+1)}\|_0 + \alpha\|G_i^{(k+1)} - f_i * J^{(k)}\|_F^2) \\ \le&c(J^{(k)}, G_1^{(k)}, G_2^{(k)}). \end{aligned}$$

By the definition of $J^{(k+1)}$,

$$\begin{aligned} &\lambda\|f_{La} * (I - J^{(k+1)})\|_F^2 + \sum_{i=1}^{2}\alpha\|G_i^{(k+1)} - f_i * J^{(k+1)}\|_F^2 \\ &\le \lambda\|f_{La} * (I - J^{(k)})\|_F^2 + \sum_{i=1}^{2}\alpha\|G_i^{(k+1)} - f_i * J^{(k)}\|_F^2. \end{aligned}$$

Thus, $c(J^{(k)}, G_1^{(k+1)}, G_2^{(k+1)}) \le c(J^{(k)}, G_1^{(k+1)}, G_2^{(k+1)}) \le c(J^{(k+1)}, G_1^{(k+1)}, G_2^{(k+1)})$. Hence, the conclusion holds. Since $c(J, G_1, G_2) \ge 0$ is a lower bounded function, HQS will converge by iteration.

IV. Experimental Results

To verify the effectiveness of the proposed dehazing method, we test it on various hazy images and compare its performance with state-of-the-art methods. When experimenting with other methods, we used the original codes provided by the

This article has been accepted for publication in a future issue of this journal, but has not been fully edited. Content may change prior to final publication. Citation information: DOI 10.1109/TCSVT.2021.3114601, IEEE Transactions on Circuits and Systems for Video Technology

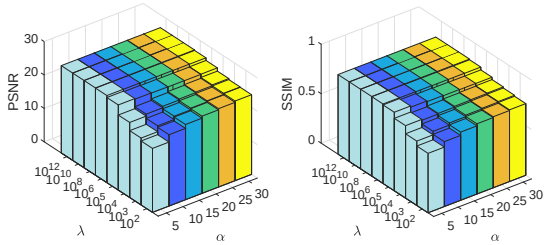

Fig. 3. (a) and (b) present the PSNR and SSIM of our method on dataset HSTS when λ varies from 10^2 to 10^{12} and α varies from 5 to 30.

authors on their websites. We show the quantitative comparisons using synthetic images and the qualitative comparisons using both synthetic and real-world images. Moreover, we perform experiments to assess the sensitivity of the algorithm HSP to parameter changes. The hardware used for Matlab code is an Intel Xeon CPU E5-2630 v4 @ 2.20 GHz with 128G RAM, and the testing software is MATLAB R2017a. Python code is executed on a PC with Intel Xeon Silver 4114 CPU, 32GB RAM, and an NVIDIA Tesla P100 GPU.

A. Analysis of Parameter Sensitivity

To explore how the parameter values affect the experimental results, we conduct several experiments with different parameters on Hybrid Subjective Testing Set (HSTS) [26]. As illustrated in Fig. 3 (a) and (b), with α fixed, the values of PSNR and SSIM are excellent when $\lambda \in (10^2, 10^{12})$. This result also coincides with the foregoing discussion that λ should be a large value. On the other hand, if λ is fixed to a larger value, the results are still satisfactory. All values of α in the range (5, 30) yield good results. It is apparent that good results are obtained for a wide range of parameter values.

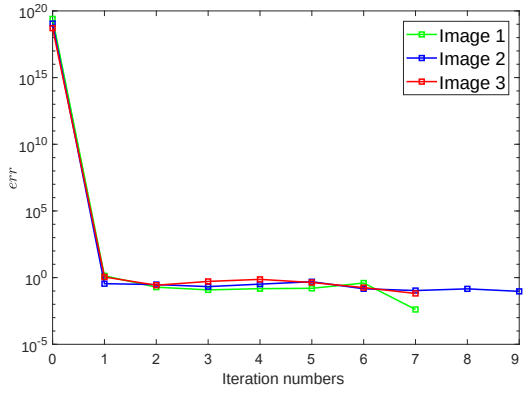

Fig. 4. The err varies with the increase of iterations number. Note the err refer to the distance between the recovered image and corresponding ground-truth.

B. Analysis of Convergence

To demonstrate the convergence of HSP intuitively, we test the proposed algorithm 1 on the first three images in Synthetic Objective Testing Set (SOTS) [26] to observe the relationship between err and the iteration number of the algorithm 1. In our experiments, τ and κ are set as 0.1 and 500, respectively. α and λ are tuned to the best. From Fig. 4, the stopping criterion in the algorithm is met within 10 times iteration. The comparison results are shown in Fig. 4, it is demonstrated experimentally that this algorithm is convergent and converges quite fast in the context of this paper.

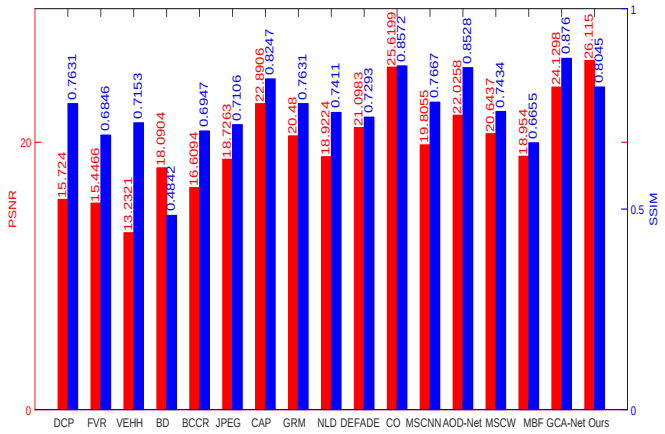

Fig. 5. Quantitative results on dataset HSTS. The histogram gives the PSNR and SSIM results of all compared methods. The red bins and blue bins represent PSNR and SSIM, respectively.

C. Explanation of Run Time

We also test the run time of our method and compare it with that of other methods. The comparisons are made using the average time for processing ten images from HSTS. The run times are measured in seconds. The experimental results are given in Table I. To show the table neatly, we omit the large run time of BD, namely 392.952s. Table I shows that our method has a longer run time than CNN-based methods (*e.g.,* MSCNN [44], AOD-Net [39], GCA-Net [47]). However, our method has a simple model, a convergent algorithm, and better dehazing results. Some other methods require a training process in advance, *e.g.,* CAP [25], AOD-Net [39] and GCA-Net [47]. Once the parameters are obtained by training, the clear image can be calculated in terms of the traditional optical model. However, their results depend strongly on the training set. For this reason, their results tend to be less effective than ours in dehazing dense haze.

D. Experiments on Synthetic Images

To measure the performance of HSP, we compare its dehazing effect with state-of-the-art dehazing methods qualitatively and quantitatively. We use HSTS [26] and NTIRE2018-Dehazing challenge datasets [55] in this section. HSTS includes 10 haze-free images and their corresponding simulated hazy images. The NTIRE2018-Dehazing challenge dataset contains an indoor dataset (*i.e.,* I-HAZE [56]) and an outdoor one (*i.e.,* O-HAZE [56]). I-HAZE contains 35 image pairs of hazy and ground-truth indoor images, and images in O-HAZE

[1] The method noted with star (*) indicates that the method is tested on the PC with GPU.

This article has been accepted for publication in a future issue of this journal, but has not been fully edited. Content may change prior to final publication. Citation information: DOI 10.1109/TCSVT.2021.3114601, IEEE Transactions on Circuits and Systems for Video Technology

TABLE I
THE TABULATION GIVES THE AVERAGE RUN TIME OF ALL COMPARED METHODS ON HSTS.

Method	DCP	FVR	VEHH	BCCR	JPEG	CAP	GRM	NLD
Run time (sec.)	0.4956	7.6768	7.8614	2.1601	0.6243	0.8423	78.9422	5.3667
Method	DEFADE	CO	MSCNN	AOD-Net* [1]	MSCW	MBF	GCA-Net* [1]	Ours
Run time (sec.)	15.4484	1.4702	1.9802	0.4026	0.3603	0.9266	0.8473	4.0521

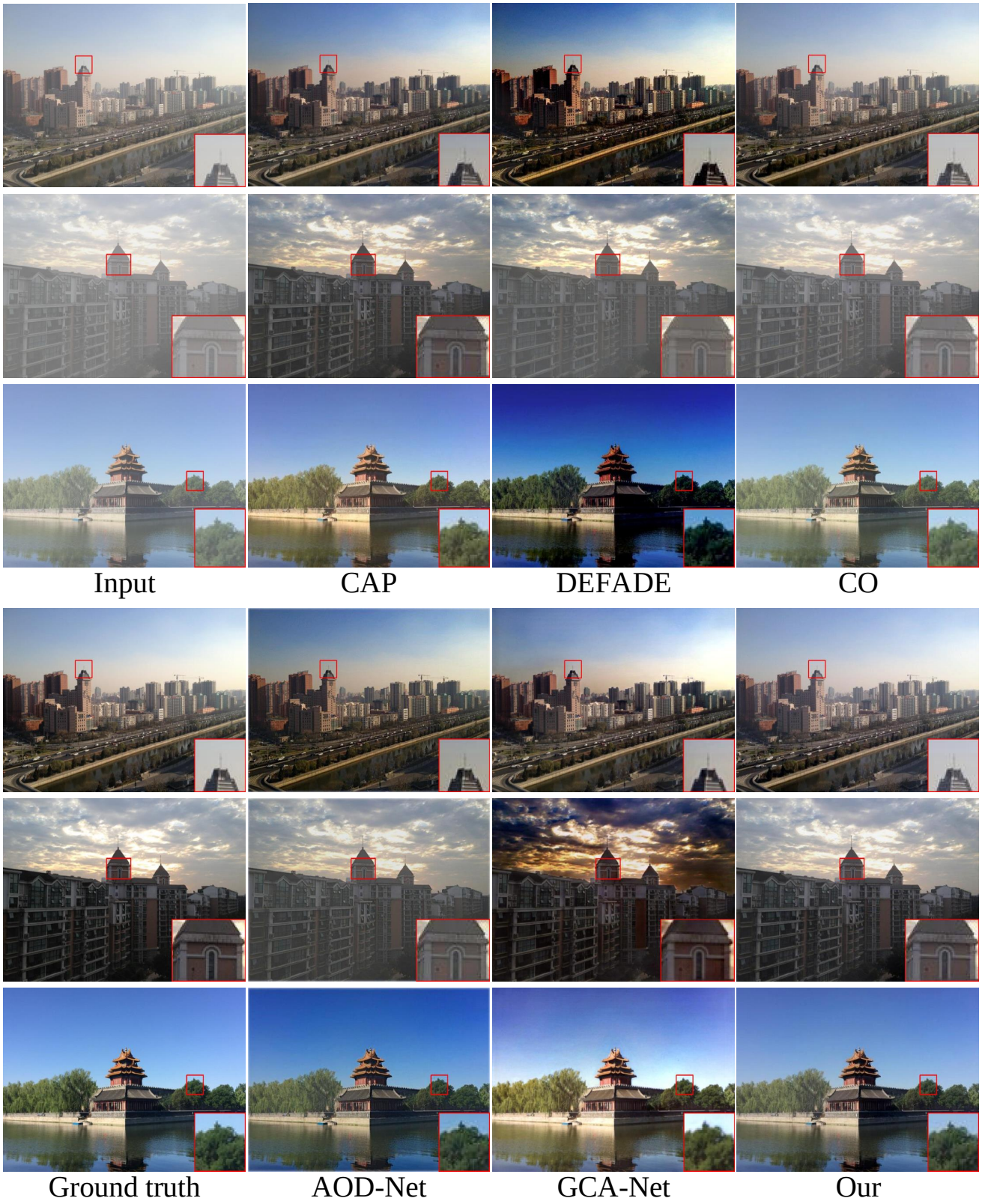

Fig. 6. The qualitative comparison on HSTS.

This article has been accepted for publication in a future issue of this journal, but has not been fully edited. Content may change prior to final publication. Citation information: DOI 10.1109/TCSVT.2021.3114601, IEEE Transactions on Circuits and Systems for Video Technology

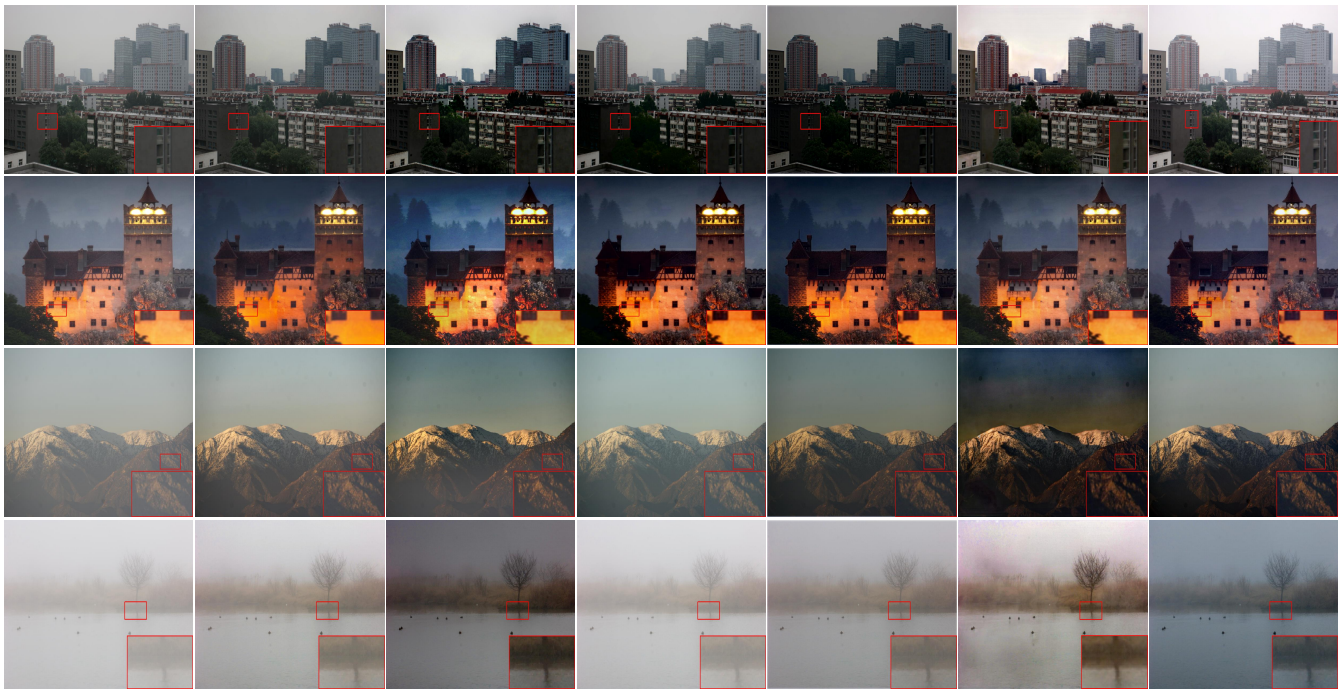

(a) Input (b) CAP (c) DEFADE (d) CO (e) AOD-Net (f) GCA-Net (g) Our

Fig. 7. The qualitative comparison on real-world images.

(a) Input (b) CAP (c) DEFADE (d) CO (e) AOD-Net (f) GCA-Net (g) Our

Fig. 8. The qualitative comparison on dense fog images. From left to right: Input image, results of CAP, results of DEFADE, results of CO, results of AOD-Net, results of GCA-Net and our dehazing results.

This article has been accepted for publication in a future issue of this journal, but has not been fully edited. Content may change prior to final publication. Citation information: DOI 10.1109/TCSVT.2021.3114601, IEEE Transactions on Circuits and Systems for Video Technology

TABLE II
QUANTITATIVE EVALUATIONS ON I-HAZE AND O-HAZE DATASETS. THE BEST AND THE SECOND-BEST RESULTS ARE MARKED IN RED AND BLUE TEXT, RESPECTIVELY. ↑ (↓) INDICATES THAT HIGH (LOW) SCORES ARE ASSOCIATED WITH BETTER PERFORMANCE.

Method	I-HAZE			O-HAZE		
	PSNR↑	SSIM↑	CIEDE2000↓	PSNR↑	SSIM↑	CIEDE2000↓
DCP	14.7953	0.7453	15.5283	16.6127	0.6480	16.1012
FVR	13.5185	0.6293	18.8705	13.7966	0.6003	20.0573
VEHH	10.5111	0.6382	23.3095	11.0676	0.5540	24.1579
BD	14.5317	0.6462	16.0886	16.5898	0.6395	16.5062
BCCR	12.7036	0.6626	18.9769	14.4333	0.5838	19.5974
JEPG	10.5687	0.5370	23.7474	12.7581	0.4180	22.9194
GRM	13.9848	0.7347	16.3440	17.9980	0.6513	14.3981
NLD	12.2870	0.6197	19.2540	15.3416	0.5907	16.5731
DEFADE	14.4913	0.6760	17.4810	15.6984	0.5958	19.5723
CO	15.7341	0.7473	13.0615	18.1326	0.6562	13.0159
MSCNN	15.2381	0.7216	15.1170	17.4513	0.6582	14.9580
AOD-Net	15.4063	0.7393	15.1502	15.0286	0.5719	19.3900
MSCW	12.9619	0.6198	18.1597	15.0905	0.6061	17.6598
MBF	14.8742	0.5280	15.6300	16.4526	0.5305	14.9396
GCA-Net	13.3634	0.6880	18.3284	17.8329	0.6530	13.7001
CAP	15.7526	0.7473	14.5848	17.3529	0.6428	14.2710
BPPNet	22.5600	0.8994	–	24.2700	0.8919	–
Ours	16.2414	0.7545	12.9326	19.0681	0.6668	11.1774

are from 45 different outdoor scenes. These two datasets are more challenging than HSTS. The experimental results are described below.

First, we compare the dehazed results on HSTS using two assessment indices PSNR and SSIM. Fig. 5 shows the PSNR and SSIM comparisons of our method with 16 state-of-the-art methods. Fig. 5 illustrates that our method achieves the highest PSNR and competitive SSIM. Second, focusing on the PSNR, we select the top six methods for a qualitative comparison. These six methods are CAP [25], DEFADE [9], CO [31], AOD-Net[39], GCA-Net [47] and our method. We choose three images, as shown in Fig. 6, for the comparison. The results of DEFADE and GCA-Net are over-saturated. As can be seen from the sky in the third image, the dehazing result of GCA-Net also suffers from a severe color shift. CAP produces excellent results in general, but there is a color shift in the restored images. For AOD-Net and CO methods, it is seen that there still exists some fog in the second picture to some extend. In comparison, our approach is able to produce better dehazing results.

To further verify the effectiveness of the proposed method, we evaluate our algorithm against all comparative approaches on more challenging datasets. We adopt the metrics PSNR, SSIM, and CIEDE2000 [57] to evaluate the quality of recovered images. Quantitative results are shown in Table II. The digital values are the averages of the results on I-HAZE and O-HAZE datasets in terms of PSNR, SSIM, and CIEDE2000. It can be seen that our proposed algorithm outperforms most previous dehazing methods by a large margin in terms of PSNR, SSIM, and CIEDE2000 on both I-HAZE and O-HAZE datasets. Although the performance of the proposed method is worse than the recent start-of-the-art CNN-based method BPPNet [58], the proposed method outperforms most state-of-the-art dehazing approaches. Compared with learning-based methods, the proposed model does not rely on large amounts of data and does not require training. Our model thus does not depend on data and computing resources. It can be easily plugged into the state-of-the-art dehazing algorithms in engineering applications. For example, it can be used as a baseline for initializing more complex dehazing methods or a guideline for beginners and engineers in this field.

E. Experiments on Real-world Images

Experiments are conducted to show the effectiveness of our method on real-world hazy images and images obtained in dense fog. Some test images are from datasets provided by [28] and [26], and others are downloaded from the Internet. The methods CAP, DEFADE, CO, AOD-Net, GCA-Net are still chosen for this comparison.

Fig. 7 shows various dehazed results on real-world images. The results of CAP, DEFADE, CO, and AOD-Net for the top image in Fig. 7 suffer from over-saturation, which produces a dimming effect. When there is lamplight in the input, as shown in the second row, apart from GCA-Net and Ours, all other approaches tend to strengthen the lamplight. The third row in Fig. 7 shows that there are varying degrees of fog in the results of CAP, DEFADE, CO, and AOD-Net. GCA-Net and Ours achieve excellent dehazing results. However, we observe that the sky regions in the third and fourth images of GCA-Net suffer from severe color shifts. In particular, the sky appears to be pink in the bottom row of GCA-Net in Fig. 7.

Fig. 8 compares images taken in dense fog. For the top row in Fig. 8, CAP, GCA-Net, and our method obtain better results than the others. However, GCA-Net suffers from the color shift. In the second row, CAP, DEFADE, AOD-Net, and GCA-Net produce unnatural colors in the sky region. All their results tend to be dark. For the third row with lamplight, the compared methods tend to strengthen the light, whereas our method can alleviate the effect of the light. In addition, we see in the third row's red box that the details for our method in the dark regions are clearer than all other compared methods. For the bottom row in Fig. 8, it is apparent that only GCA-Net and our method are effective in eliminating fog. As a consequence, it is demonstrated that our method is effective for dense fog images and achieves the best results as compared with the state-of-the-art methods.

V. Conclusion

In this paper, we have presented a novel additive model for dehazing. It can effectively characterize the relation between the clear image and the corresponding haze image layer. In addition, a powerful haze smoothness prior is introduced to constrain this model. The proposed single image dehazing method has been tested on both synthetic images and real-world images. Extensive experimental results and comparisons show that the proposed method produces satisfactory results, especially for dense fog removal. In future research, we will explore other problems that may benefit from our method and explore an even better dehazing approach by combining the prior in this work with the neural network method.

Acknowledgement

This work was supported in part by the National Natural Science Foundation of China [grant nos. 61922064, U2033210], in part by the Zhejiang Provincial Natural Science Foundation [grant nos. LR17F030001, LQ19F020005], in part by the Project of science and technology plans of Wenzhou City [grant no. C20170008].

References

[1] H. Koschmieder, "Theorie der horizontalen sichtweite," *Beitrage zur Physik der freien Atmosphare*, pp. 33–53, 1924.

[2] Y. Y. Schechner, S. G. Narasimhan, and S. K. Nayar, "Instant dehazing of images using polarization," in *IEEE Conference on Computer Vision and Pattern Recognition*, 2001, pp. 325–332.

[3] Schechner, Yoav Y and Narasimhan, Srinivasa G and Nayar, Shree K, "Polarization-based vision through haze," *Applied optics*, vol. 42, no. 3, pp. 511–525, 2003.

[4] S. G. Narasimhan and S. K. Nayar, "Chromatic framework for vision in bad weather," in *IEEE Conference on Computer Vision and Pattern Recognition*, 2000, pp. 598–605.

[5] S. K. Nayar and S. G. Narasimhan, "Vision in bad weather," in *IEEE International Conference on Computer Vision*, 1999, pp. 820–827.

[6] S. G. Narasimhan and S. K. Nayar, "Contrast restoration of weather degraded images," *IEEE Transactions on Pattern Analysis and Machine Intelligence*, vol. 25, no. 6, pp. 713–724, 2003.

[7] R. Fattal, "Single image dehazing," *ACM Transactions on Graphics*, vol. 27, no. 3, pp. 1–9, 2008.

[8] R. T. Tan, "Visibility in bad weather from a single image," in *IEEE Conference on Computer Vision and Pattern Recognition*, 2008, pp. 1–8.

[9] L. K. Choi, J. You, and A. C. Bovik, "Referenceless prediction of perceptual fog density and perceptual image defogging," *IEEE Transactions on Image Processing*, vol. 24, no. 11, pp. 3888–3901, 2015.

[10] A. Galdran, J. Vazquez-Corral, D. Pardo, and M. Bertalmio, "Enhanced variational image dehazing," *SIAM Journal on Imaging Sciences*, vol. 8, no. 3, pp. 1519–1546, 2015.

[11] R. Luzón-González, J. L. Nieves, and J. Romero, "Recovering of weather degraded images based on rgb response ratio constancy," *Applied Optics*, vol. 54, no. 4, pp. B222–B231, 2015.

[12] K. He, J. Sun, and X. Tang, "Single image haze removal using dark channel prior," *IEEE Transactions on Pattern Analysis and Machine Intelligence*, vol. 33, no. 12, pp. 2341–2353, 2010.

[13] S.-C. Pei and T.-Y. Lee, "Nighttime haze removal using color transfer pre-processing and dark channel prior," in *IEEE International Conference on Image Processing*, 2012, pp. 957–960.

[14] K. B. Gibson, D. T. Vo, and T. Q. Nguyen, "An investigation of dehazing effects on image and video coding," *IEEE Transactions on Image Processing*, vol. 21, no. 2, pp. 662–673, 2011.

[15] B. Xie, F. Guo, and Z. Cai, "Improved single image dehazing using dark channel prior and multi-scale retinex," in *International Conference on Intelligent System Design and Engineering Application*, 2010, pp. 848–851.

[16] Q. Zhu, S. Yang, P. A. Heng, and X. Li, "An adaptive and effective single image dehazing algorithm based on dark channel prior," in *IEEE International Conference on Robotics and Biomimetics*, 2013, pp. 1796–1800.

[17] C. Xiao and J. Gan, "Fast image dehazing using guided joint bilateral filter," *The Visual Computer*, vol. 28, no. 6-8, pp. 713–721, 2012.

[18] Y. Xiang, R. R. Sahay, and M. S. Kankanhalli, "Hazy image enhancement based on the full-saturation assumption," in *IEEE International Conference on Multimedia and Expo Workshops*, 2013, pp. 1–4.

[19] J.-P. Tarel and N. Hautiere, "Fast visibility restoration from a single color or gray level image," in *IEEE International Conference on Computer Vision*, 2009, pp. 2201–2208.

[20] J.-P. Tarel, N. Hautiere, L. Caraffa, and A. Cord, "Vision enhancement in homogeneous and heterogeneous fog," *IEEE Intelligent Transportation Systems Magazine*, vol. 4, no. 2, pp. 6–20, 2012.

[21] K. He, J. Sun, and X. Tang, "Guided image filtering," *IEEE Transactions on Pattern Analysis and Machine Intelligence*, vol. 35, no. 6, pp. 1397–1409, 2012.

[22] G. Meng, Y. Wang, J. Duan, S. Xiang, and C. Pan, "Efficient image dehazing with boundary constraint and contextual regularization," in *IEEE International Conference on Computer Vision*, 2013, pp. 617–624.

[23] J.-S. Lee, C.-H. Li, and H.-Y. Lee, "Visibility dehazing based on channel-weighted analysis and illumination tuning," *Multimedia Tools and Applications*, vol. 78, no. 2, pp. 1831–1856, 2019.

[24] C. O. Ancuti, C. Ancuti, C. Hermans, and P. Bekaert, "A fast semi-inverse approach to detect and remove the haze from a single image," in *Asian Conference on Computer Vision*, 2010, pp. 501–514.

[25] Q. Zhu, J. Mai, and L. Shao, "A fast single image haze removal algorithm using color attenuation prior," *IEEE Transactions on Image Processing*, vol. 24, no. 11, pp. 3522–3533, 2015.

[26] B. Li, W. Ren, D. Fu, D. Tao, D. Feng, W. Zeng, and Z. Wang, "Benchmarking single-image dehazing and beyond," *IEEE Transactions on Image Processing*, vol. 28, no. 1, pp. 492–505, 2018.

[27] K. Nishino, L. Kratz, and S. Lombardi, "Bayesian defogging," *International Journal of Computer Vision*, vol. 98, no. 3, pp. 263–278, 2012.

[28] R. Fattal, "Dehazing using color-lines," *ACM Transactions on Graphics*, vol. 34, no. 1, pp. 1–14, 2014.

[29] D. Berman, S. Avidan *et al.*, "Non-local image dehazing," in *IEEE Conference on Computer Vision and Pattern Recognition*, 2016, pp. 1674–1682.

[30] D. Berman, T. Treibitz, and S. Avidan, "Air-light estimation using haze-lines," in *IEEE International Conference on Computational Photography*, 2017, pp. 1–9.

[31] J. He, C. Zhang, R. Yang, and K. Zhu, "Convex optimization for fast image dehazing," in *IEEE International Conference on Image Processing*, 2016, pp. 2246–2250.

[32] Y. Li, F. Guo, R. T. Tan, and M. S. Brown, "A contrast enhancement framework with jpeg artifacts suppression," in *European Conference on Computer Vision*, 2014, pp. 174–188.

[33] C. Chen, M. N. Do, and J. Wang, "Robust image and video dehazing with visual artifact suppression via gradient residual minimization," in *European Conference on Computer Vision*, 2016, pp. 576–591.

[34] M. Ju, C. Ding, Y. J. Guo, and D. Zhang, "Idgcp: Image dehazing based on gamma correction prior," *IEEE Transactions on Image Processing*, vol. 29, pp. 3104–3118, 2019.

[35] M. Ju, C. Ding, W. Ren, Y. Yang, D. Zhang, and Y. J. Guo, "Ide: Image dehazing and exposure using an enhanced atmospheric

scattering model," *IEEE Transactions on Image Processing*, vol. 30, pp. 2180–2192, 2021.
[36] J. Zhang, Y. Cao, S. Fang, Y. Kang, and C. Wen Chen, "Fast haze removal for nighttime image using maximum reflectance prior," in *IEEE Conference on Computer Vision and Pattern Recognition*, 2017, pp. 7418–7426.
[37] J. Zhang, Y. Cao, Z.-J. Zha, and D. Tao, "Nighttime dehazing with a synthetic benchmark," in *Proceedings of the ACM International Conference on Multimedia*, 2020, pp. 2355–2363.
[38] X. Zhang, T. Wang, J. Wang, G. Tang, and L. Zhao, "Pyramid channel-based feature attention network for image dehazing," *Computer Vision and Image Understanding*, vol. 197, p. 103003, 2020.
[39] B. Li, X. Peng, Z. Wang, J. Xu, and D. Feng, "Aod-net: All-in-one dehazing network," in *IEEE International Conference on Computer Vision*, 2017, pp. 4770–4778.
[40] X. Zhang, T. Wang, W. Luo, and P. Huang, "Multi-level fusion and attention-guided cnn for image dehazing," *IEEE Transactions on Circuits and Systems for Video Technology*, 2020.
[41] J. Zhang and D. Tao, "Famed-net: A fast and accurate multi-scale end-to-end dehazing network," *IEEE Transactions on Image Processing*, vol. 29, pp. 72–84, 2019.
[42] T. Wang, L. Zhao, P. Huang, X. Zhang, and J. Xu, "Haze concentration adaptive network for image dehazing," *Neurocomputing*, vol. 439, pp. 75–85, 2021.
[43] X. Zhang, R. Jiang, T. Wang, and W. Luo, "Single image dehazing via dual-path recurrent network," *IEEE Transactions on Image Processing*, vol. 30, pp. 5211–5222, 2021.
[44] W. Ren, S. Liu, H. Zhang, J. Pan, X. Cao, and M.-H. Yang, "Single image dehazing via multi-scale convolutional neural networks," in *European Conference on Computer Vision*, 2016, pp. 154–169.
[45] B. Cai, X. Xu, K. Jia, C. Qing, and D. Tao, "Dehazenet: An end-to-end system for single image haze removal," *IEEE Transactions on Image Processing*, vol. 25, no. 11, pp. 5187–5198, 2016.
[46] X. Zhao, K. Wang, Y. Li, and J. Li, "Deep fully convolutional regression networks for single image haze removal," in *IEEE Visual Communications and Image Processing*, 2017, pp. 1–4.
[47] D. Chen, M. He, Q. Fan, J. Liao, L. Zhang, D. Hou, L. Yuan, and G. Hua, "Gated context aggregation network for image dehazing and deraining," in *IEEE Winter Conference on Applications of Computer Vision*, 2019, pp. 1375–1383.
[48] X. Liu, H. Zhang, Y.-m. Cheung, X. You, and Y. Y. Tang, "Efficient single image dehazing and denoising: An efficient multi-scale correlated wavelet approach," *Computer Vision and Image Understanding*, pp. 23–33, 2017.
[49] Y. Cho, J. Jeong, and A. Kim, "Model-assisted multiband fusion for single image enhancement and applications to robot vision," *IEEE Robotics and Automation Letters*, vol. 3, no. 4, pp. 2822–2829, 2018.
[50] Y. Shao, L. Li, W. Ren, C. Gao, and N. Sang, "Domain adaptation for image dehazing," in *IEEE Conference on Computer Vision and Pattern Recognition*, 2020, pp. 2808–2817.
[51] Y. Li and M. S. Brown, "Single image layer separation using relative smoothness," in *IEEE Conference on Computer Vision and Pattern Recognition*, 2014, pp. 2752–2759.
[52] A. Levin and Y. Weiss, "User assisted separation of reflections from a single image using a sparsity prior," *IEEE Transactions on Pattern Analysis and Machine Intelligence*, vol. 29, no. 9, pp. 1647–1654, 2007.
[53] R. C. Gonzalez, R. E. Woods, and B. R. Masters, "Digital image processing, third edition," *Journal of Biomedical Optics*, vol. 14, no. 2, 2009.
[54] L. Xu, S. Zheng, and J. Jia, "Unnatural ℓ_0 sparse representation for natural image deblurring," in *IEEE Conference on Computer Vision and Pattern Recognition*, 2013, pp. 1107–1114.
[55] C. Ancuti, C. O. Ancuti, and R. Timofte, "Ntire 2018 challenge on image dehazing: Methods and results," in *IEEE Conference on Computer Vision and Pattern Recognition Workshops*, 2018, pp. 891–901.
[56] C. Ancuti, C. O. Ancuti, R. Timofte, and C. De Vleeschouwer, "I-haze: a dehazing benchmark with real hazy and haze-free indoor images," in *International Conference on Advanced Concepts for Intelligent Vision Systems*, 2018, pp. 620–631.
[57] Y. Zhang, Y. Tian, Y. Kong, B. Zhong, and Y. Fu, "Residual dense network for image super-resolution," in *IEEE Conference on Computer Vision and Pattern Recognition*, 2018, pp. 2472–2481.
[58] A. Singh, A. Bhave, and D. K. Prasad, "Single image dehazing for a variety of haze scenarios using back projected pyramid network," in *European Conference on Computer Vision*, 2020, pp. 166–181.

Xiaoqin Zhang received the B.Sc. degree in electronic information science and technology from Central South University, China, in 2005 and Ph.D. degree in pattern recognition and intelligent system from the National Laboratory of Pattern Recognition, Institute of Automation, Chinese Academy of Sciences, China, in 2010. He is currently a professor in Wenzhou University, China. His research interests are in pattern recognition, computer vision and machine learning. He has published more than 80 papers in international and national journals, and international conferences, including IEEE T-PAMI, IJCV, IEEE T-IP, IEEE T-IE, IEEE T-C, ICCV, CVPR, NIPS, IJCAI, AAAI, and among others.

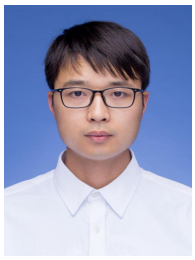

Tao Wang received his M.Sc. from the College of Computer Science and Artificial Intelligence, Wenzhou University, China, in 2021 and the B.Sc. degree in information and computing science from Hainan Normal University, China, in 2018. His research interests include several topics in computer vision and machine learning, such as object tracking/detection, image/video quality restoration, adversarial learning, image-to-image translation and reinforcement learning.

Guiying Tang received her M.S. degree from the College of Mathematics and Physics, Wenzhou University, China in 2020 and B.Sc. degree in the College of Mathematics and Software Science, Sichuan Normal University, China, in 2017. Her main research interest is in computer vision and deep learning, such as image quality restoration, object tracking.

Li Zhao received the B.Sc. degree in automation in 2005 and MEng degree in control theory and control engineering in 2008 from Central South University, China. She is currently an assitant researcher in Wenzhou University. Her research interests are in pattern recognition, computer vision, and machine learning.

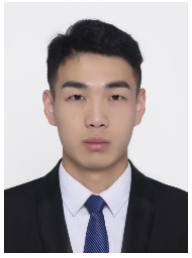

Yuewang Xu is currently a graduate student at the College of Computer Science and Artificial Intelligence, Wenzhou University, China. He received the B.Sc. degree in computer science and technology from Shandong University of Technology, China, in 2020. His research interests include several topics in computer vision and machine learning, such as salient object detection, image/video super resolution, and recommendation algorithm.

Steve Maybank received the B.A. degree in mathematics from King's College, Cambridge, MA, in 1976, and the Ph.D. degree in computer science from Birkbeck College, University of London, London, UK, in 1988. In 1980, he was with the Pattern Recognition Group, Marconi Command and Control Systems, Frimley, London, UK. In 1989, he was with the GEC Hirst Research Centre, Wembley, London. From 1993 to 1995, he was a Royal Society/Engineering and Physical Sciences Research Council Industrial Fellow with the Department of Engineering Science, University of Oxford, Oxford, UK. In 1995, he was a lecturer with the Department of Computer Science, University of Reading, Reading, UK. In 2004, he joined as a professor with the School of Computer Science and Information Systems, Birkbeck College, London. His current research interests include the geometry of multiple images, camera calibration, visual surveillance, information geometry, and the applications of statistics to computer vision.